Electron Paramagnetic Resonance Investigation of the Structure of Graphene Oxide: pH dependence of the spectroscopic response

Bin Wang,[†] *Alistair J. Fielding*[§*] *and Robert A. W. Dryfe*[†*]

[†]School of Chemistry, University of Manchester, Oxford Road, Manchester M13 9PL, United Kingdom

[§]School of Pharmacy and Biomolecular Science, Liverpool John Moores University, James Parsons Building, Byrom Street, Liverpool, L3 3AF, United Kingdom.

To whom correspondence should be addressed.

Emails: a.j.fielding@ljmu.ac.uk ; robert.dryfe@manchester.ac.uk

ABSTRACT

The time dependence of the electron paramagnetic resonance (EPR) signal arising from purified graphene oxide (GO) in various solvents has been investigated. The prepared GO was sequentially base and acid (ba) treated to remove manganese impurities. The EPR signal of ba-GO was found to be pH dependent, when exposed to different aqueous solutions, which is related to the de-carboxylation process the material undergoes in solution. This process involves the fragmentation of the carbonaceous framework, and occurs most rapidly in alkaline conditions. Under acidic conditions, fragmentation is much slower, leading to a gradual increase in the EPR signal from ba-GO in the presence of oxygen. Inferred structural changes were correlated with those deduced from X-ray photoelectron spectroscopy to explain the observed pH and time-dependent effects. Comparative experiments showed that the oxygen molecule was the key to the increase of unpaired electron density. Exposure to superoxide anions *in situ* confirmed the scavenging ability of ba-GO was related to the oxidation of the sp^2 carbon structure, which led to an increase of the EPR signal. Overall, the results demonstrate changes of the structure and stability of GO at different pH values.

KEYWORDS: Graphene Oxide, Electron Paramagnetic Resonance, Structure, pH dependence

Graphene oxide (GO) is a two-dimensional form of carbon with a high proportion of oxygen functionalized groups on both its basal plane and edges.[1, 2] Unlike its "parent" material, graphene, the high oxygen content renders it hydrophilic and it is therefore readily dispersed in aqueous solutions. These properties have led to many different applications of this material being proposed. For example, GO can serve both as a supporting framework for various inorganic/organic active species [3-5] as well as a useful material for applications such as drug delivery and for the development of biosensors.[6-7] Moreover, GO can be easily transformed into paper-like materials[8-11] with important applications in filtration and separation, and its oxygen functional groups make its use in different fields, such as water treatment,[8] photoluminescence[12] catalysis,[13-16] and optoelectronics,[13] possible. In spite of the plethora of work on the applications of this material, certain properties of GO are still quite poorly understood.[17]

Much of the structural information on GO is derived from seminal nuclear magnetic resonance (NMR) studies, notably the Lerf-Klinowski model, where the oxygen functionalities of the parent graphite oxide were identified.[18-19] Electron paramagnetic resonance (EPR) spectroscopy is a sensitive method to study carbon-related materials, as it can provide detailed information about the characteristics of different paramagnetic species.[20-24] Somewhat surprisingly, in view of the importance of NMR in understanding the structure and reactivity of GO, EPR studies of this material are limited. To the best of our knowledge, the first EPR study of GO was carried out by Szabó *et al.*[25] and the origin of the spins has often been assigned to localized free radicals associated with lattice defects.[26-31] As well as a narrow signal, Su *et al*.[23] found a broad EPR signal, attributed to the π electrons on the edge states of nanographene, which are believed to play an important role in the generation of superoxide anions during catalytic processes. The broad signal caused by π electrons is also found in reduced GO materials.[27, 32, 33] Interestingly,

Qiu *et al.*[34] found that graphene related materials can be used as antioxidants and are highly effective as hydroxyl radical scavengers. They found that few-layer graphene is more active than GO in radical scavenging, which led to the suggestion that the trapping property was linked to the sp^2-carbon network. Hou *et al.*[29] realized control over the radicals species in graphene oxide by photo-irradiation or reduction processes.[35] They suggested the formation of radicals was associated with homolytic bond scission of oxygen-containing functional groups.

Herein, the time-dependent EPR behaviour of the ba-GO film has been studied in both acidic and basic aqueous media. The purpose of giving GO the sequential base and acid wash was to separate oxidative debris and metallic contamination (see Scheme 1 and Figure S1 in Supporting Information), which could otherwise interfere with the EPR response due to their high unpaired electron content, not least because of the transition metals used as oxidizing agents in the preparation of GO.[36] In order to avoid the non-resonant microwave absorption caused by the aqueous solution, the rolled ba-GO membrane was put in a capillary to monitor the EPR behaviour in different solution environments. Markedly different behavior was found when ba-GO was exposed to aqueous solutions of different pH. Spectral simulation and XPS analysis were used to rationalize the observations. Finally, the spin trapping ability of ba-GO was found to increase the spin concentration of GO.

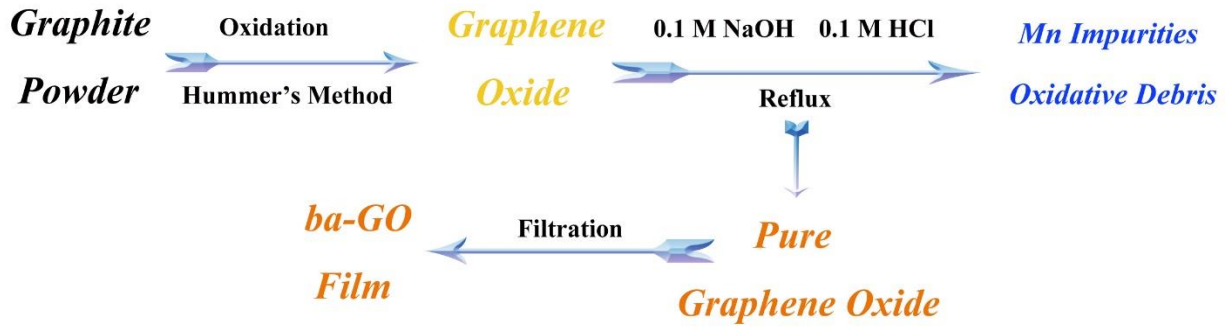

Scheme 1. Preparation of ba-GO film with the base and acid wash to remove impurities.

Results

As shown in Figure 1a, the EPR signal of solid ba-GO can be fitted to two curves both with g values around 2.0028: a narrow Lorentzian curve (linewidth of 2.7 G, 78 %) and a broader Lorentzian curve (linewidth ~11 G, 22 %). The narrow signal has been widely considered to come from localized sigma electrons at defects.[23, 26-31, 37] The broad signal has been related to conductive π-carriers propagating in the extended aromatic graphite like structure. The fast spin-lattice relaxation through interaction with adjacant π-electron systems leads to a broader line width.[23, 32, 38, 39] The EPR signal of ba-GO film was found to be pH dependent (Figure 1b) when exposed to different solutions, with the greatest signal observed at pH 14 (1 M KOH solution) and the weakest signal by a factor of four found at pH 0.4 (1 M H_2SO_4 solution). This is in accord with previous literature, which has demonstrated that the EPR signal from GO is markedly increased after exposure to hydroxide solutions.[40] When the sample was dispersed in H_2SO_4, it is notable that the broad component falls to around 9 % compared to the solid state (Figure 1c), while it was absent in 1 M KOH (Figure 1d). Also, the EPR signal at 9 and 35 GHz from the ba-GO films was found to be isotropic in the aqueous solvents (Figure S2).

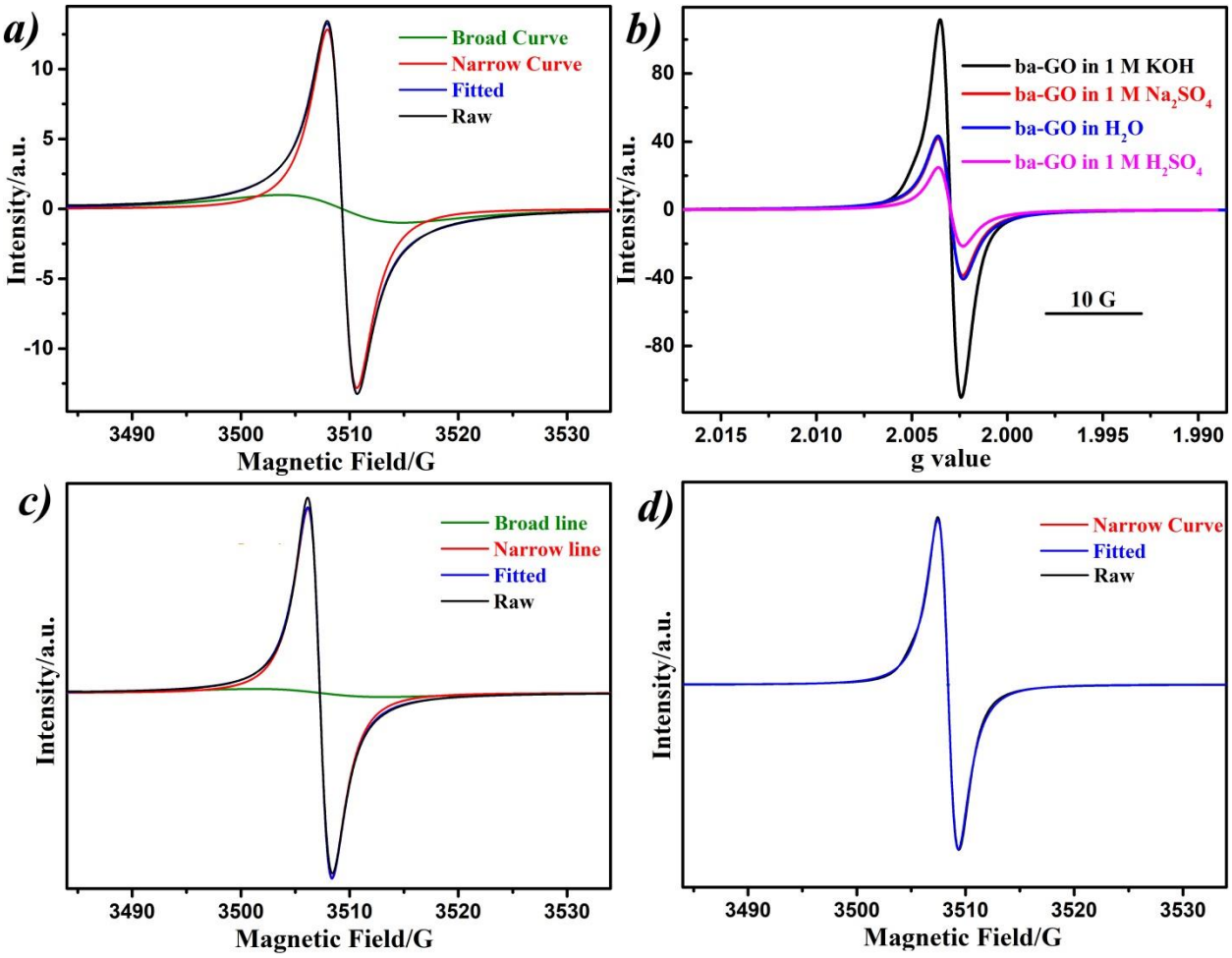

Figure 1. a) EPR signal and simulation of the ba-GO film; b) EPR signal of the ba-GO film (1 mg) in different aqueous solutions; c) EPR simulation of ba-GO exposed to 1 M H_2SO_4; d) EPR simulation of ba-GO exposed to 1 M KOH.

Figure 2 shows the time-dependence of the EPR spectrum of the ba-GO film when exposed to 1 M H_2SO_4 and 1 M KOH, respectively. All control experiments (such as the response from the aqueous solvents or PTFE alone, which are shown in Figure S3) were EPR silent. Thus, the change illustrated in Figure 2 was due to the ba-GO film itself. As with the initial signal, the EPR spectral change of ba-GO with time was dependent on the pH of the aqueous medium. The peak-to-peak amplitude changes are shown in Figure 3 and based on the first EPR signal recorded after an exposure time of 2 minutes. In 1 M H_2SO_4, the EPR signal of ba-GO increased over

time, as shown in Figure 3a, the signal increased by 33 % after 170 h with the fastest rate of change at the beginning. During the exposure process, the proportion of broad component decreased, along with the growth of the narrow component (Figure 3b). By contrast, in 1 M KOH, the EPR signal intensity and double integration value of the ba-GO film decayed over time: only 60 % of the spins remained after exposure for 170 h in 1 M KOH. Interestingly, there was no obvious difference of the peak-to-peak width of the EPR signal when ba-GO was exposed to the solutions over time, indicating the nature of the spins kept the same (as shown in S4).

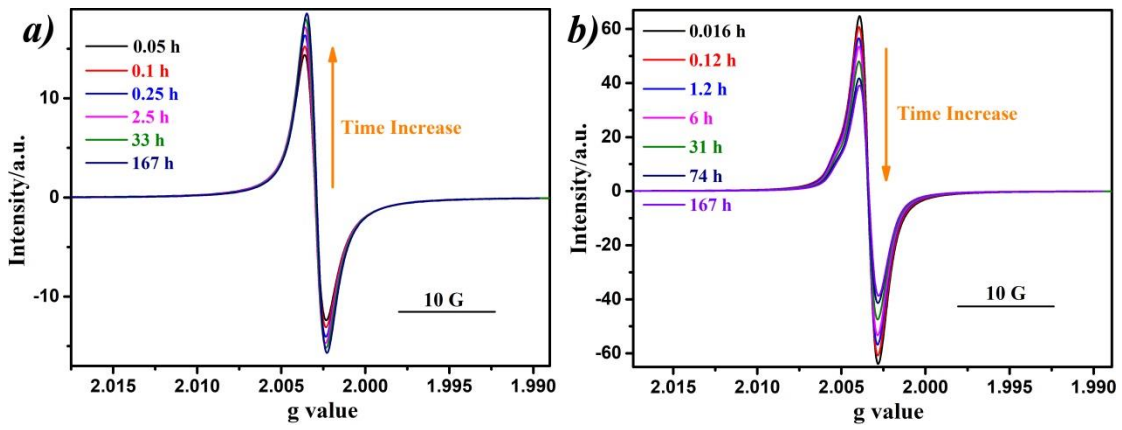

Figure 2. EPR spectrum change over time when the ba-GO film (1 mg) was exposed to 1 M H_2SO_4 (a) and 1 M KOH (b).

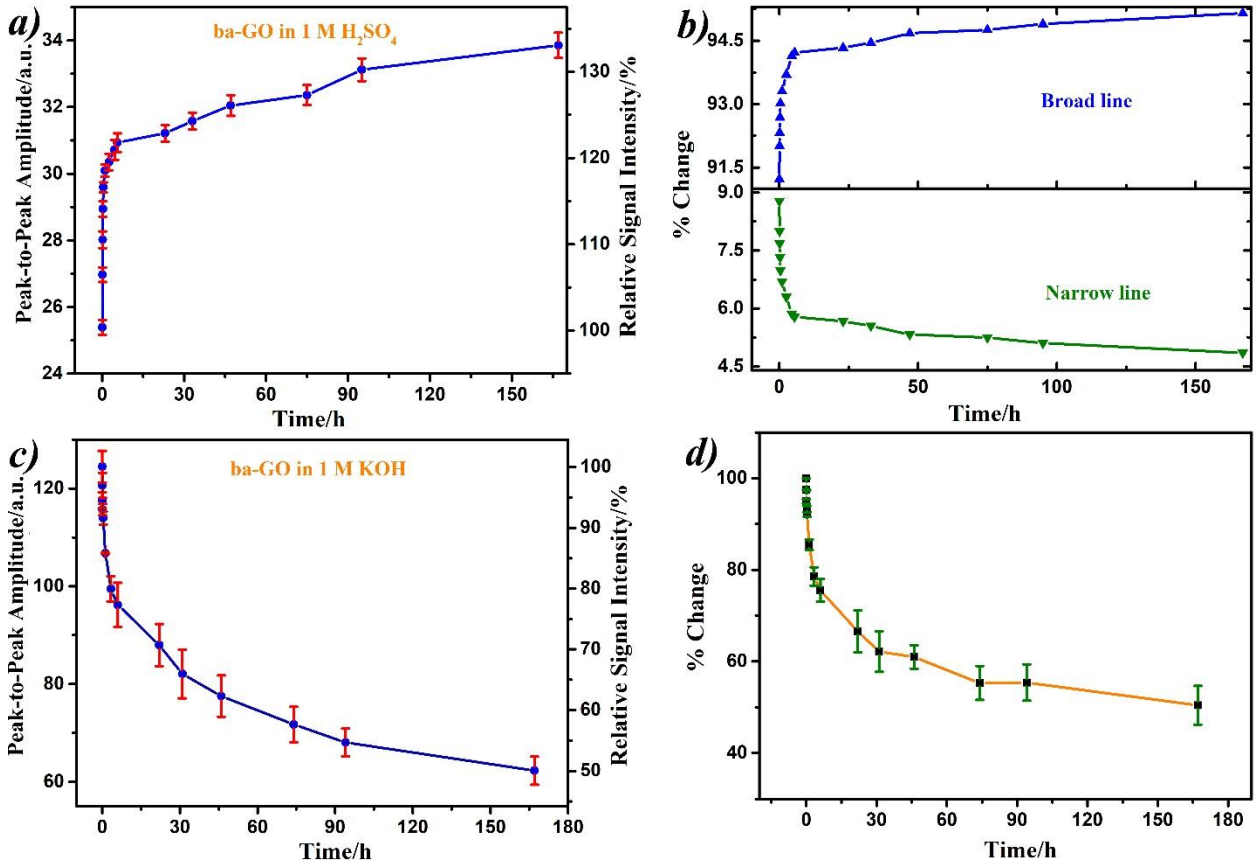

Figure 3. Time-dependent EPR change of ba-GO film in different aqueous solutions. (a) The signal amplitude change and (b) the % change of the broad and the narrow components over time in 1 M H_2SO_4; (c) the signal amplitude change and (d) and the relative percentage change of the double integrated value over time of ba-GO exposed in 1 M KOH.

When the time-dependent experiment in 1 M H_2SO_4 was carried out under anaerobic conditions, the EPR signal did not show sustained growth (Figure S5a,b). Both the narrow signal and the broad component decreased over time, indicating that O_2 is responsible for the EPR signal increase in 1 M H_2SO_4 under aerobic conditions.

Figure 4 displays the C1s XPS spectra of the ba-GO film with different exposure times in aqueous solvents. C1s spectra present four carbon atom environments corresponding to different functional groups: the non-oxygenated ring C, and the carbon associated with C–O bonds, the

carbonyl (C=O), and the carboxylate (O–C=O) groups, respectively.[41-43] The change of functional groups under each of the employed conditions is given in Table 1. When exposed to 1 M H_2SO_4 (Figure 4a), the ba-GO sp^2 carbon component decreased over time, accompanied with a slight increase in the C-OH/COOH groups. These results are consistent with an increase in oxidation when the carbon material was exposed to acidic conditions.[44-46] In contrast, in KOH (Figure 4c,d), both the sp^2 carbon and the carbonyl component increased over time, while the hydroxyl groups (C-OH) decreased over time. This observation is consistent with the mechanism discussed by Tour *et al*., who proposed that deoxygenation of GO in alkaline conditions could form –C=O groups and, ultimately, decrease the oxygen content of the solid.[47] The infrared spectroscopy of ba-GO after different exposure times is shown in Figure S6 and supported the XPS results. A slight increase of –COOH and –OH was found in H_2SO_4 over the exposure time, while the decrease of $–CO^-$ and $–COO^-$ was found when the exposure time in KOH was increased.[48]

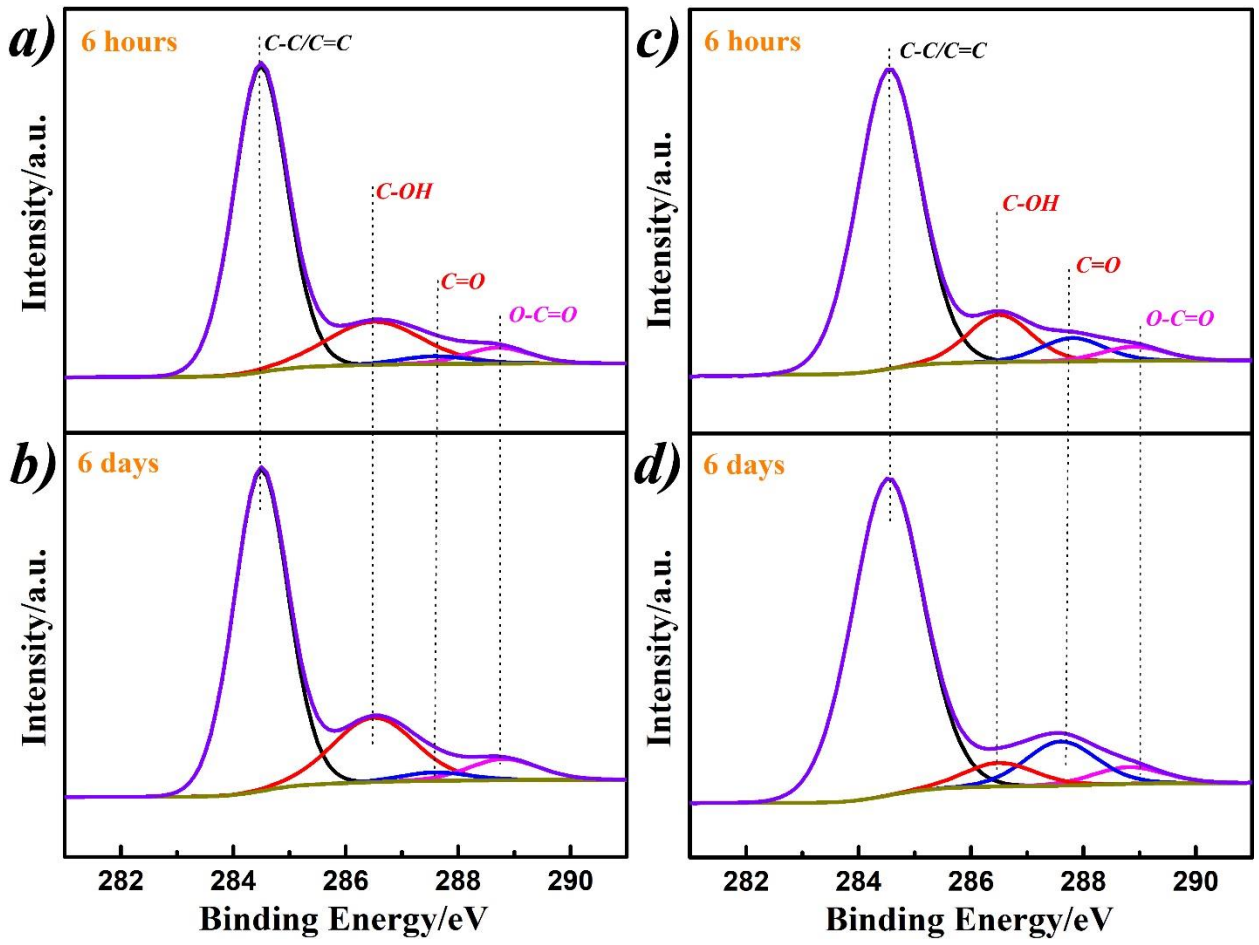

Figure 4. Comparison of C(1s) XPS data of the ba-GO film with different exposure times. ba-GO film exposed to 1 M H_2SO_4 for (a) 6 h and (b) 6 days; ba-GO film exposed to 1 M KOH for (c) 6 h and (d) 6 days.

Table 1. XPS component analysis of the ba-GO film as a function of exposure time.

ba-GO		*C content*	*C=C/C-C*	*C-O*	*C=O*	*OCO*
H_2SO_4 (1 M)	6 h	81.6 %	71.8 %	21.6 %	2.2 %	4.4 %
	6 days	73.4 %	69.0 %	22.5 %	2.1 %	6.4 %
KOH	*6 h*	85.3 %	77.8 %	12 .3%	6.0 %	3.9 %

(1 M)	6 days	87.0 %	79.6 %	6.0 %	10.6 %	3.8%

In order to understand further the nature of the spin environment, the temperature dependent EPR behavior of the ba-GO film with, and without, solution exposure treatment was investigated (Figure 5). For ba-GO in the solid state (Figure 5a), the narrow component obeys the Curie-Weiss Law, which is consistent with localized defect states such as sigma dangling spins.[33, 49] While the broad component was only found at the higher temperature range, and was temperature independent (Pauli Law). This is indicative of delocalized π electrons interacting within the extended π electron system. After the ba-GO film was exposed to different solutions for 24 hours, the EPR signal still obeyed the Curie-Weiss Law (Figure 5b) with little variation between the samples. The line width was also found to be temperature dependent (Figure S7) and decreased on raising the temperature. This has been observed previously and related to a narrowing mechanism associated with edge states.[27]

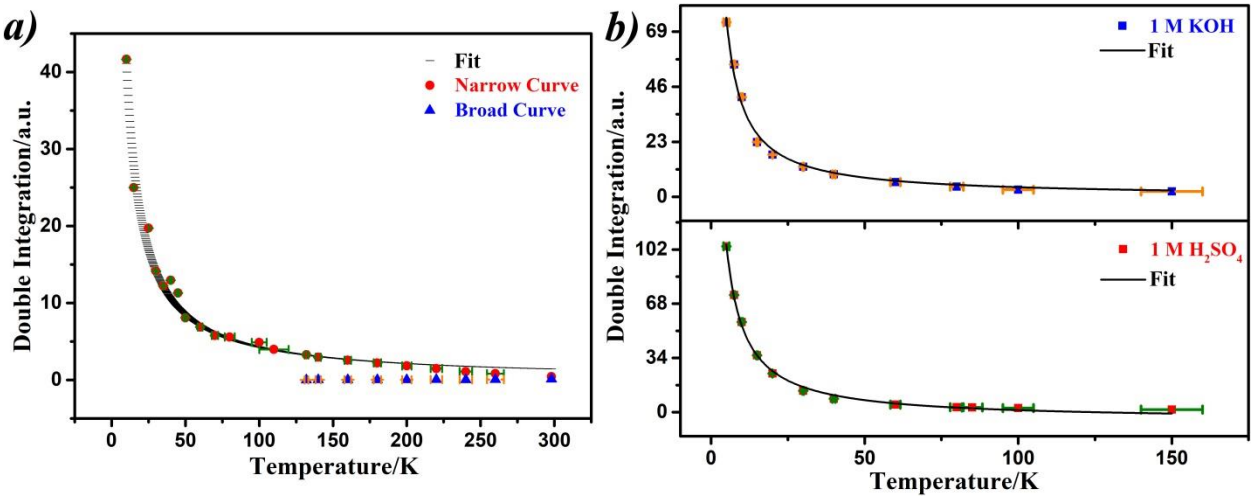

Figure 5. Temperature dependence of (a) solid ba-GO film and (b) after 24-hour exposure to different solutions. The data was fit using the Curie-Weiss law as described in the experimental section.

The spin behaviour of the GO film was further studied through experiments in the presence of superoxide. Figure 6a shows the time dependent behaviour of ba-GO film during exposure to superoxide radicals. Superoxide was generated by using the β nicotinamide adenine dinucleotide 2′-phosphate reduced tetrasodium salt hydrate (NADH) and phenazinemethosulfate (PMS) reaction system (N/P) in phosphate buffer pH 7.4 (Figure S8).[34, 50] The narrow component of the EPR signal of ba-GO film increased on exposure to superoxide-rich solutions (Figure 6b). When the concentration of superoxide radical was increased, the maximum EPR signal of ba-GO increased (Figure 6b); indicating the scavenging of superoxide radicals by ba-GO leads to a higher density of localized sigma unpaired electrons.

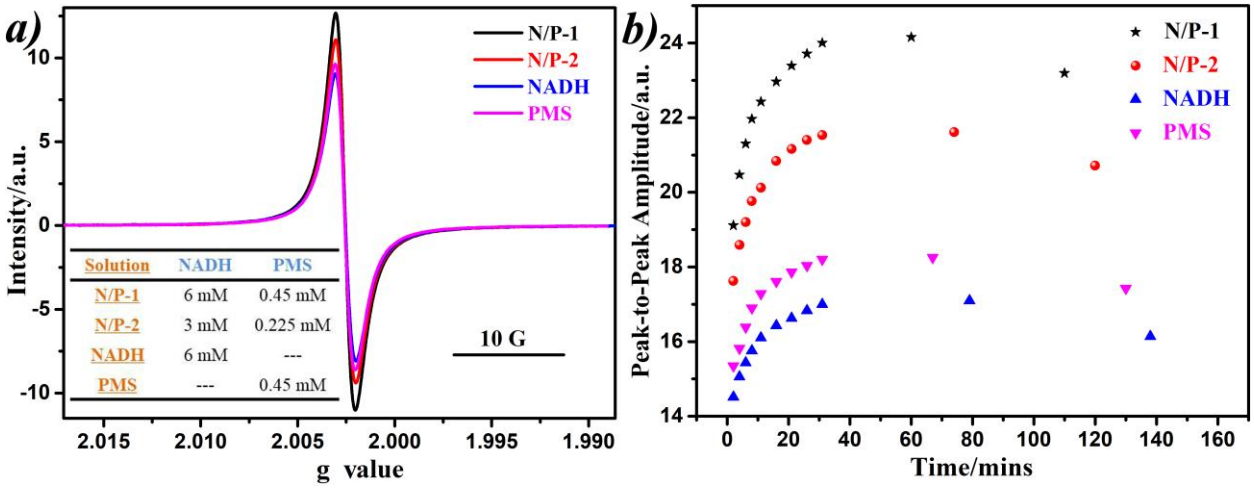

Figure. 6. a) Comparison of the EPR signal of the ba-GO film in NADH/PMS reaction system with different concentrations; b) Time dependent EPR behavior of ba-GO film in NADH/PMS reaction system with different concentrations.

Discussion

The graphene oxide material was free from Mn residues derived from the Hummers method of preparation: in general, EPR is a useful method to detect the presence of manganese impurities.[51] Graphene oxide samples, without the initial base washing procedure, contained a high level of

Mn^{2+} impurities, which were easily detected by the EPR method (Figure S1). The EPR signal of GO has been described as a narrow Lorentzian curve, derived from C centered radicals present at defects.[23, 26-31] However, in the case of the ba-GO studied here, a broader component, which is related to π electrons, was also found. This should be related to the additional purification process. The removal of oxygen-containing functional groups (such as hydroxyl, carboxyl, Figure S9) and the recovery of the sp^2 structure reconstitutes more aromatic units at the edge, which create favorable conditions for the existence of delocalized π electron density.[23]

The magnetic property of graphene based materials is strongly related to edge states. Enoki *et al*.[38] studied activated carbon fibers as model systems for investigating the magnetism of edge-state spins and showed that magnetic properties change as a result of temperature of treatment, as thermal treatment removes functional groups and creates more electron transport path networks. The nature of spins changed from localized states to itinerant ones, as observed through the temperature dependence of the magnetic susceptibility; Curie-Weis behavior from localized edge-state spins to the less temperature dependent susceptibility of conduction electrons. Non-bonding π electrons trapped by the defects such as zigzag edge states and vacancies show a Curie like behavior.[37-39] GO has similar structure as to nanographene, while the edge state is more complicated than graphene. However, oxidation and reduction of GO coupled with EPR can offer information about the sites of the paramagnetism. Szabó *et al*.[25] found that the EPR signal of GO became weaker and even disappeared when the GO was further oxidized. They attributed the EPR signal of GO to arise from mobile π electrons that are stabilized by the resonance energy in the condensed aromatic structure rather than from broken bonds. Zahra *et al*.[31] found that UVA irradiation and chemical reduction with ascorbic acid produce smaller amounts of radicals on reduced GO nanosheets. Erdem *et al*.[22] found that chemical reduction of GO removed

most oxygen-containing functionalities restoring the graphene lattice and as a consequence quenched the EPR signal through the reduced the local spin-state density. Residual EPR signal was attributed to defect centers from zigzag edges of graphene planes.

We now attempt to relate the differing EPR behavior of ba-GO film in aqueous solutions of varying pH to the associated structural changes. The pH dependence of signal intensity (Figure 1b) is interpreted as a manifestation of the de-carboxylation in different aqueous solutions. The work of Dimiev *et al*.[47] indicates that exposure of GO to alkaline solutions effectively leads to a disproportionation with respect to oxidized carbons, with two alcohol groups being converted into half an equivalent C=C unit and a ketone group. Under more extreme (temperature/pH) conditions, this process leads to a loss of carbon dioxide. GO is a relatively acidic material (pKa values: 4.3 for carboxylic groups and 9.8 for phenolic OH).[48] We therefore attribute the initial high unpaired electron density in KOH solution, as seen in the EPR data of Figures 1, to the generation of carboxyl type radical species, formed from the fragmentation (and associated oxidation) of GO at high pH. As fragmentation proceeds, however, the de-carboxylation of this material removes the sources of stabilized unpaired electron density, and the EPR signal falls rapidly with time (Figure 3). By contrast, under acidic conditions in the presence of oxygen, although the protons can initiate the oxidative degradation of GO, the associated generation of protons on decomposition slows down the cleavage of the material, meaning that simultaneous generation and consumption of "edge" functional groups, which are the locus of unpaired electrons, is slowed down. This means that the initial unpaired density is much lower, but slowly increases, as the oxidative fragmentation of the material proceeds at a much slower rate, in accord with the EPR data of Figures 1-3. The XPS data shown in Table 1 is also consistent with the hypothesized increase in carboxyl functional groups, and associated decrease of hydroxyl

groups (see Figure 4c,d). This loss of electron-withdrawing functional groups, which are likely to stabilize unpaired electron density, explains why the signal intensity falls.

The radical scavenging ability of ba-GO was verified by the superoxide generation experiment shown in Figure 6a,b. The radical scavenging mainly reflected an increase of the narrow component (Figure 6a), indicating the creation of σ type "dangling bond" spins at defects. The known chemistry of superoxide suggests a mechanism associated with electron transfer or adduct formation.[34, 52, 53] The oxidation may proceed via an initial abstraction of labile hydrogen atoms by the superoxide radical anion resulting in a radical and HOO^-, which should be more favored in polar solvent.[54] However, it is not possible to rule out acting as a nucleophile and attacking the activated double bonds of the GO surface to produce a radical adduct stabilized by the conjugation of the GO surface. Itkis *et al*.[55, 56] recent XPS studies confirmed superoxide species could cause carbon-to-carbonate transformation inside an electrochemical cell.

Conclusion

Graphene oxide, prepared the from Hummers' method, was subjected to a prolonged base and acid wash to remove both magnetic impurities and oxidative debris. The resulting solid, ba-GO, has two EPR components, attributed to localized sigma dangling bond spins and delocalized π electrons which interact with the aromatic structure inside the flake. The narrow EPR signal of ba-GO was found to decrease over time in KOH and increase over time in H_2SO_4 in the presence of oxygen. The radical quench in KOH was related to loss of electron-withdrawing functional groups from the deoxygenation process. Under acidic conditions, this oxidative fragmentation is much slower, leading to a gradual increase in the EPR signal from ba-GO in the presence of oxygen. The comparison to XPS results and the anaerobic control test in H_2SO_4 confirmed the

increase of oxygen content. Superoxide radicals were found to cause an increase of the narrow component of the EPR signal, although further experiments (e.g. involving XPS) are needed to confirm the mechanism. Finally, the experiments serve as a useful guide to the stability of ba-GO at different pH values for future application.

MATERIALS & METHODS

All chemicals were of analytical grade and were used without further purification.

ba-GO. GO was synthesized from graphite flake (~325 mesh, from Sigma-Aldrich) by the modified Hummer's method.[57] First, graphite powder (5 g) was mixed with concentrated sulfuric acid (115 mL) and then stirred in an ice bath for 50 mins. To keep the temperature below 10 ºC, 25 g $KMnO_4$ was slowly added under continued stirring. The mixture was stirred under the ice bath for a further 2.5 h, then the reaction mixture was warmed to 35 ºC and the temperature kept constant for 45 mins. Then, 400 mL deionized water was added and the temperature increased to 70 ºC. After 15 mins, another 300 mL of deionized water was added. Finally, 36 g of 30 % H_2O_2 was added to remove excess $KMnO_4$. The mixture was centrifuged and washed with 5 % HCl and deionized water several times, and further dialysed for more than one month to remove impurities. Physical washing such as filtration and dialysis cannot remove manganese impurities completely.[21, 22, 50] The as-produced GO was further treated with the base and the acid solution, previously reported in the literature to remove residual manganese ions.[23, 36] Specifically, GO (1 mg/mL) was refluxed at 100 ºC in 0.1 M NaOH (aq.) for 1 h, then the treated GO was separated by filtration. The product obtained was dissolved in 0.1 M HCl (aq.) followed by reflux at 100 ºC for 1h. The final product, ba-GO, was filtered and washed with H_2O. This base-acid treatment of GO removes manganese impurities/oxidative debris derived from the initial Hummers'

oxidation. The EPR signal of the Mn^{2+} in the initially prepared GO could be detected easily (Figure SI-1), whereas after the base-acid wash, no Mn^{2+} signal was found in the EPR signal. Moreover, an inductively coupled plasma mass spectrometry analysis of the sample failed to detect Mn impurities (the manufacturer quoted a detection limit of Mn is 0.07 μg/L).[58]

ba-GO Films. ba-GO film was prepared by filtration. The ba-GO powder was dispersed in water and sonicated for 2 hours to yield a suspension. Polytetrafluoroethylene (PTFE) membranes (25 mm diameter hydrophilic PTFE membrane filter with a 0.1 μm pore size and thickness of 140 μm, purchased from Merck Millipore) were used as the support to make the film, as they are flexible enough to roll into a columnar-like shape.

Characterization methods. X-ray photoelectron spectroscopy (XPS) measurements were performed on an ESCALAB 250Xi spectrometer (ThermoFisher-VG Scientific) using a monochromated Al Ka X-ray source (1486.6 eV). Transmission electron microscopy (TEM) measurements were carried out using Thermo Scientific (FEI) Talos F200X instrument. The average flake size of GO sheets was 1-5 μm^2.

Time-dependent EPR behaviour. The EPR signal arising from the ba-GO film in aqueous solutions was recorded in continuous-wave (CW) at 9 GHz (X-band) using a Bruker Micro spectrometer. The ba-GO film (*ca*. 1 mg) was rolled into a cylindrical shape and then plugged into a capillary (1 mm) filled with aqueous solution. Triplicate samples were made. All EPR experiments were carried out at room temperature with a modulation amplitude of 1 G, microwave power of 2 mW, and the spectra reported herein were typically the average of 20 scans. Q band (35 GHz) EPR experiments were carried using a Bruker EMX spectrometer at room temperature. DPPH radical was used as a magnetic field standard. All EPR experiments were measured under unsaturated conditions as shown in Figure SI-10.

The experiments to study the influence of oxygen in acidic solution was carried out as follows: The solution was bubbled with Argon gas for more than 1 hour, and then the film was left under vacuum (relative vacuum: −30 kPa) for 24 hours. The sample was placed into a capillary inside a glove box, and then the capillary was sealed with glue.

The formula of the Lorentzian absorption lineshape used to simulate the spectra was:

$$f_L(x) = \frac{2}{\pi\sqrt{3}}\frac{1}{\Gamma}\left[1+\frac{4}{3}\left(\frac{x-x_0}{\Gamma}\right)^2\right]^{-1}$$

where x_0 is the center, Γ is related to the FWHM (full width at half height): FWHM= $\Gamma/\sqrt{3}$.

The temperature dependent data (Figure 5) was fitted by using the Curie-Weiss law: $X_{EPR} = C/(T-T_0)$. X_{EPR} stands for the spin susceptibility, and here we use the double integration value of the EPR signal; C is the Curie constant; T is the measured temperature and T_0 is the Curie-Weiss temperature (T_0 = -6.97 K).

Superoxide radical capture experiment. The generation of superoxide anions used an NADH/PMS solution.[34, 49] Typically, NADH and PMS were both dissolved in phosphate buffered saline (PBS) (pH 7.4). The operation and the testing conditions were the same as described above. The amount of superoxide anions was adjusted by changing the concentration of the NADH/PMS solution. The generation mechanism of superoxide radical production is shown in Figure S7.

Associated Content

Supporting Information.

EPR detection of Mn impurities; Multifrequency EPR measurements; EPR background measurements; EPR spectral change over time and temperature in acidic and alkaline aqueous;

Mechanism of superoxide generation; Comparison of C 1s XPS of GO and ba-GO. This is available free of charge on the ACS publications website at… .

Acknowledgement

We thank the National EPSRC EPR service and Facility for support (NS/A000055/1) and EPSRC (UK) for funding (EP/K016954/1, EP/I023879/1). B.W. thanks the President's Doctoral Scholarship from the University of Manchester. We also acknowledge great technical assistance from Mr. Adam Brookfield and the useful mechanism discussion with Jiangnan Li.

Competing Interests

The authors declare no competing interests.

References

1. Stankovich, S; Dikin, D. A.; Dommett, G. H. B.; Kohlaas, K. M.; Zimney, E. J.; Stach, E. A.; Piner, R. D.; Nguyen, S. T. and Ruoff, R. S. Graphene-based composite materials. *Nature*, **2006**, 442, 282-286.

2. Zhu, Y. W.; Murali, S.; Cai, W. W.; Li, X. S.; Suk, J. W.; Potts, J. R. and Ruoff, R. S. Graphene and Graphene Oxide: Synthesis, Properties, and Applications. *Adv. Mater.*, **2010**, 22, 3906-3924.

3. Chen, S.; Wu, J.; Wu, X.; Han Q. and Wang X. Graphene oxide-MnO_2 nanocomposites for supercapacitors. *ACS Nano*, **2010**, 4, 2822-2830

4. Scheuermann, G. M.; Rumi, L.; Steurer, P.; Bannwarth W. and Mulhaupt R. Palladium Nanoparticles on Graphite Oxide and Its Functionalized Graphene Derivatives as Highly Active Catalysts for the Suzuki−Miyaura Coupling Reaction. *J. Am. Chem. Soc.*, **2009**, 131, 8262-8270

5. Wu, Z.; Zhou, G.; Yin, L.; Ren, W.; Li, F. and Cheng, H. M. Graphehe.metal oxide composite electrode materials for energy storage. *Nano Energy*, **2012**, 1, 107-131

6. Sun, X.; Liu, Z.; Welsher, K.; Robinson, J.; Goodwin, A.; Zaric, S. and Dai, H. J. Nano-graphene oxide for cellular imaging and drug delivery. *Nano Res.*, **2008**, 1, 203-212

7. Chung, C.; Kim, Y. K.; Shin, D.; Ryoo, S. R.; Hong, B. H. and Min, D. H. Biomedical application of graphene and graphene oxide. *Acc. Chem. Res.*, 2013, 45, 2211-2224.

8. Nair, R. R.; Wu, H. A.; Jayaram, P. N.; Grigorieva I. V. and Geim, A.K. Unimpeded permeation of water through Helium-Leak–Tight graphene-based membranes. *Science*, **2012**, 335, 442-444.

9. Eda, G.; Chhowalla. M.; Chemically derived graphene oxide: towards large-area thin-film electronics and optoelectronics. *Adv. Mater.*, **2010**, 22, 2392-2415.

10. Dikin, D .A.; Stankovich, S.; Zimney, E. J.; Piner, R .D.; Dommett, G.; Evmenenko, G.; Nguyen, S. T. and Ruoff, R. S. Preparation and characterization of graphene oxide paper. *Nature*, **2007**, 448, 457-460.

11. Mei, Q. S.; Zhang, Z. P. Photoluminescent graphene oxide ink to print sensors onto microporous membranes for versatile visualization bioaasays. *Angew. Chem. Int. Ed.*, **2012**, 51, 5602-5606.

12. Mei, Q. S.; Zhang, K.; Guan, G J.; Liu, B. H.; Wang, S. H. and Zhang, Z. P. Highly efficient photoluminescent graphene oxide with tunable surface properties. *Chem. Commun.*, **2010**, 46, 7319-7321.

13. Song, Y. J.; Qu, K. G.; Zhao, C.; Ren, J. S. and Qu, X. G. Graphene oxide: intrinsic peroxidase catalytic activity and its application to glucose detection. *Adv. Mater.*, **2010, 22**, 2206-2210.

14. Boukhvalov, D. W.; Dreyer, D. R.; Bielawski, C. W. and Son, Y. W. A computational investigation of the catalytic properties of graphene oxide: exploring mechanisms by using DFT Methods. *ChemCatChem*, **2012**, 2, 1844-1849.

15. Dreyer, D.R.; Jia, H. P. and Bielawski, C. W. Graphene oxide: a convenient carbocatalyst for facilitating oxidation and hydration reactions. *Angew. Chem. Int. Ed.*, **2010**, 49, 6813-6816.

16. Dreyer, D.R. and Bielawski, C. W. Carbocatalysis: Heterogeneous carbons finding utility in synthetic chemistry. *Chem. Sci.*, **2011**, 2, 1233-1240.

17. Yang, L.; Zhang, R.; Liu, B.; Wang, J.; Wang, S.; Han, M. and Zhang, Z. P. π-conjugated carbon radicals at graphene oxide to initiate ultrastrong chemiluminescence. *Angew. Chem. Int. Ed.*, **2014**, 53, 10109-10113.

18. Lerf, A.; He, H.; Forester, M. and Klinowski, J. Structure of graphite oxide revisited. *J. Phys. Chem. B*, **1998102**, 4477-4482.

19. Gao, W.; Alemany, L.B.; Ci, L. and Ajayan, P. M. New insights into the structure and reduction of graphite oxide. *Nat. Chem.*, **2009**, 1, 403-408.

20. Zaka, M.; Ito, Y.; Wang, H.; Yan, W.; Robertson, A.; Wu, Y. A.; Rümmeli, M. H.; Staunton, D.; Hashimoto, T.; Morton, J. J. L.; Ardavan, A.; Briggs, G. A. D. and Warner, J. H. Electron paramagnetic resonance investigation of purified catalyst-free single-walled carbon nanotubes. *ACS Nano*, **2010**, 4, 7708-7716.

21. Tampieri, F.; Silvestrini, S.; Ricco, R.; Maggini, M. and Barbon, A. A comparative electron paramagnetic resonance study of expanded graphites and graphene. *J. Mater. Chem. C*, 2014, 2, 8105-8112.

22. Pham, C. V.; Krueger, M.; Eck, M.; Weber, S. and Erdem, E. Comparative electron paramagnetic resonance investigation of reduced graphene oxide and carbon nanotubes with different chemical functionalities for quantum dot attachment. *Appl. Phys. Lett.*, **2014**, 104, 132102.

23. Su, C.; Acik, M.; Takai, K.; Lu, J.; Hao, S.j.; Zheng, Y.; Wu, P.; Bao, Q.; Enoki, T.; Chabal, Y. J. and Loh, K. P. Probing the catalytic activity of porous graphene oxide and the origin of this behavior. *Nat.Commun.*, **2012**, 3, 1298.

24. Stathi, P.; Gournis, D.; Deligiannakis, Y. and Rudolf, P. Stabilization of phenolic radicals on graphene oxide: an XPS and EPR study. *Langmuir*, **2015**, 31, 10508-10516.

25. Szabó, T.; Berkesi, O.; Forgó, P.; Josepovits, K.; Sanakis, Y.; Petridis, D. and Dékány, I. Evolution of Surface Functional Groups in a Series of Progressively Oxidized Graphite Oxides. *Chem. Mater.*, **2006**, 18, 2740–2749.

26. Rao, S. S.; Stesmans, A.; Kosynkin, D. V.; Higginbotham, A. and Tour, J. M. Paramagnetic centers in graphene nanoribbons prepared from longitudinal unzipping of carbon nanotubes. *New J. Phys.*, **2011**, 12, 113004.

27. Diamantopoulou, A.; Glensi, S.; Zolnierkiwicz, G.; Guskos, N. and Likodimons, V. Magnetism in pristine and chemical reduced graphene oxide. *J. Appl. Phys.*, **2017**, 121, 043906.

28. Feng, R; Zhou, W.; Guan, G.; Li, C.; Zhang, D.; Zhang, Y.; Zheng, L. and Zhu, W. Surface decoration of graphene by grafting polymerization using graphene oxide as the initiator. *J. Mater. Chem.*, **2012**, 22, 3982-3989.

29. Hou, X. L.; Li, J. L.; Drew, S. C.; Tang, B.; Sun, L. and Wang, X. G. Tuning Radical Species in Graphene Oxide in Aqueous Solution by Photoirradiation. *J. Phys. Chem. C*, **2013**, 117, 6788–6793.

30. Ćirić, L.; Sienkiewicz, A.; Gaál, R.; Jaćimović, J.; Vâju, C.; Magrez, A and Forró, L. Defects and localization in chemically-derived graphene. *Phys. Rev. B*, **2012**, 86, 195139.

31. Nia, Z.K.; Chen, J.Y.; Tang, B.; Wang, X.G. and Li, J.L. Optimizing the free radical content of graphene oxide by controlling its reduction. *Carbon*, **2017**, 116, 703-712.

32. Rao, S. S.; Stesmans, A.; Wang, Y. and Chen, Y. Direct ESP evidence for magnetic behavior of graphite oxide. *Physica E*, **2012**, 44, 1036-1039.

33. Ćirić, L.; Sienkiewicz, A.; Djokić, D. M.; Smajda, R.; Magrez, A.; Kaspar, T.; Nesper, R. and Forró, L. Size dependence of the magnetic response of graphite oxide and graphene flakes – an electron spin resonance study. *Phys. Status Solidi B*, **2010**, 247, 2958–2961.

34. Qiu, Y.; Wang, Z.; Owens, A.; Kulaots, I.; Chen, Y.; Kane A. B. and Hurt, R. H. Antioxidant chemistry of graphene-based materials and its role in oxidation protection technology. *Nanoscale*, **2014**, 6, 11744-11755.

35. Nia, Z. K.; Chen, J. Y.; Tang, B.; Yuan, B. and Wang, X. G. Optimizing the free radical content of graphene oxide by controlling its reduction. *Carbon*, **2017**, 116, 703-712.

36. Rourke, J. P.; Pandey, P. A.; Moore, J. J.; Bates, M.; Kinloch, I. A.; Young R. J. and Wilson, N. R. The Real Graphene Oxide Revealed: Stripping the Oxidative Debris from the Graphene-like Sheets. *Angew. Chem., Int. Ed.*, **2011**, 50, 3173-3177.

37. Takai, K.; Suzuki, T.; Enoki, T.; Nishihara, H. and Kyotani, T. Structure and magnetic properties of curved graphene networks and the effects of bromine and potassium adsorption. *Phys. Rev. B*, **2010**, 81, 205420.

38. Enoki, T. and Takai, K. The edge state of nanographene and the magnetism of the edge-state spins. *Solid State Commun.*, **2009**, 149, 1144-1150.

39. Joly, V. L. J.; Takahara, K,; Takai, K,; Sugihara, K,; Enoki, T.; Koshino, M. and Tanaka, H. Effect of electron localization on the edge-state spins in a disordered network of nanographene sheets. *Phys. Rev. B*, **2010**, 81, 115408.

40. Lai, W. C.; Wang, Z. M.; Li, Y. L., Wang, X., Liu, Y. and Liu, X.Y. Radical Mechanism for the reduction of Graphene Derivatives Initiated by Electron-Transfer Reaction. *J. Phys. Chem. C*, **2018**, 122, 8473-8479.

41. Stankovich, S.; Dikin, D. A.; Piner, R. D.; Kohlhaas, K. A.; Kleinhammes, A.; Jia, Y.; Wu, Y.; Nguyen, S. T. and Ruoff, R. S. Synthesis of graphene-based nanosheets via chemical reduction of exfoliated graphite oxide. *Carbon*, **2007**, 5, 1558-1568.

42. Yan, J.; Wei, T.; Shao, B.; Ma, F. and Fan, Z. Electrochemical properties of graphene nanosheet/carbon black composites as electrodes for supercapacitors. *Carbon*, **2010**, 5, 1731-1737.

43. Yang, D.; Velamkanni, A.; Bozoklu, G.; Park, S.; Stoller, M.; Piner, R. D.; Stankovich, S.; Jung, I.; Field, D. A.; Ventrice, C. A. and Ruoff, R. S. Chemical analysis of graphene oxide films after heat and chemical treatments by X-ray photoelectron and Micro-Raman spectroscopy. *Carbon*, **2009**, 47, 145-152.

44. Datsyuk, V.; Kalyva, M.; Papagelis, K.; Parthenios, J.; Tasis, D.; Siokou, A.; Kallitsis, I.; Galiotis, C. Chemical oxidation of multiwalled carbon nanotubes. *Carbon*, **2008**, 46, 833-840.

45. Coleman, V. A.; Knut, R.; Karis, O.; Grennbery, H.; Jansson, U.; Quinlan, R.; Sanyal, B. and Eriksson, O. Defect formation in graphene nanosheets by acid treatment: an x-ray absorption spectroscopy and density functional theory study. *J. Phys. D: Appl. Phys.*, **2008**, 41, 062001.

46. Bouleghlimat, E.; Davies, P. R.; Davies, R. J.; Howarth, R.; Kulhavy, J.and Morgan, D. J. The effect of acid treatment on the surface chemistry and topography of graphite. *Carbon*, **2013**, 124-133.

47. Dimiev, A. M.; Alemany, L. B. and Tour, J. M. Graphene oxide. Origin of acidity, its instability in water and a new dynamic structure model. *ACS Nano*, **2013**, 7, 576-588.

48. Konkena, B. and Vasudevan, S. Understanding Aqueous Dispersibility of Graphene Oxide and Reduced Graphene Oxide through pKa Measurements. *J. Phys. Chem. Lett.*, **2012**, 3, 867-872.

49. Náfrádi, B.; Nemes, N. M.; Fehér, T.; Forró, L.; Kim, Y.; Fischer, J. E.; Luzzi, D. E.; Simon, F. and Kuzmany, H. Electron spin resonance of single-walled carbon nanotubes and related structures. *Phys. Status Solidi B*, **2006**, 243, 3106-3110.

50. Nimse, S. B. and Pal, D. Free radicals, natural antioxidants, and their reaction mechanisms. *RSC Adv.*, **2015**, 5, 27986-28006.

51. Panich, A. M.; Shames, A. I.; Aleksenskii, A. E. and A. Dideikin. Magnetic resonance evidence of manganese-graphene complexes in reduced graphene oxide. *Solid State Commun.*, **2012**, 152, 466-468.

52. Bitner, B.R., Marcno, D.C., Berlin, J.M., Fabian, R.H., Cherian, L., Culver, J.C., Dickinson, M.E., Robertson, C.S., Pautler, R.G., Kent, T.A. and Tour, J.M. Antioxidant carbon particles improve cerebrovascular dysfunction following traumatic brain injury. *ACS Nano*, **2012**, 6, 8007.

53. Hayyan, M.; Hashim, M.A. and AlNashef, I.M. Superoxide ion: generation and chemical implications. *Chem. Rev.*, **2016**, 116, 3029.

54. Frimer, A.A.; Faekash-Solomon, T. and Aljadeff, G. Mechanism of the superoxide anion radical ($O_2^{-\bullet}$) mediated oxidation of diarylmethanes. *J. Org. Chem.*, **1986**, 51, 2093.

55. Itkis, D. M.; Semenenko, D. A.; Kataev, E. Y.; Belova, A. I.; Neudachina, V. S.; Sirotina, A. P.; Havecker, M.; Teschner, D.; Gericke, A. Knop; P. D.; Barinov, A.; Goodilin, E. A.; Horn,

Y. S. and Yashina, L.V. Reactivity of Carbon in Lithium–Oxygen Battery Positive Electrodes. *Nano Lett.*, **2013**, 13, 4697-4701.

56. Kataev, Y. E.; Itkis, D. M.; Fedorov, A. V.; Senkovsky, B. V.; Usachov, D. Y.; Verbitskiy, N. I.; Vyalikh, D. V. and Yashina, L. V. Oxygen Reduction by Lithiated Graphene and Graphene-Based Materials. *ACS Nano*, **2015**, 9, 320-326.

57. Hummers, W. S. and Offeman, R. E. Preparation of Graphitic Oxide, *J. Am. Chem. Soc.*, **1958**, 80, 1339.

58. https://assets.thermofisher.com/TFS-Assets/CMD/Specification-Sheets/PS-43229-ICP-OES-iCAP-7200-PS43229-EN.pdf. Access date September 2018.

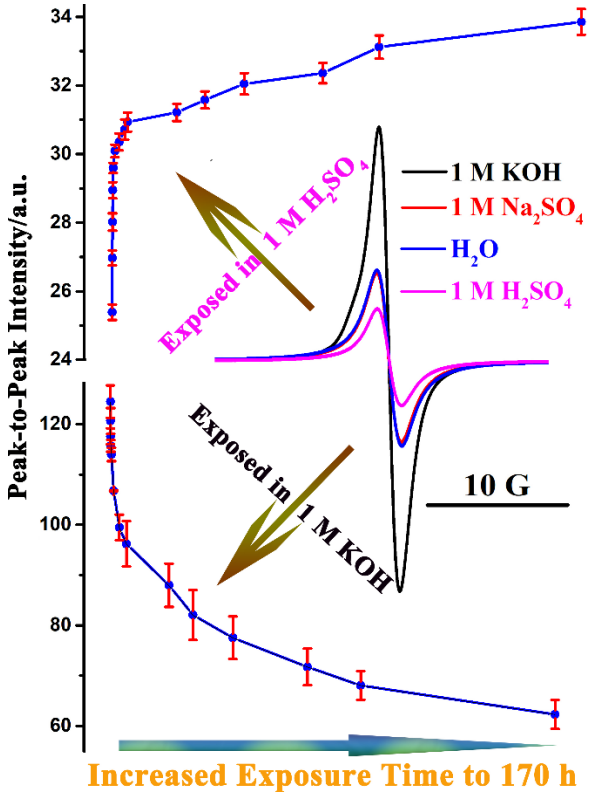
Peak-to-Peak Intensity/a.u.
34
32
30
28
26
24
120
100
80
60
Exposed in 1 M H2SO4
1 M KOH
1 M Na2SO4
H2O
1 M H2SO4
Exposed in 1 M KOH
10 G
Increased Exposure Time to 170 h

1

2